SCANNING VOL. 23, 182–192 (2001)

Received: May 30, 2000
Accepted with revision: July 27, 2000

Mapping Piezoelectric-Field Distribution in Gallium Nitride with Scanning Second-Harmonic Generation Microscopy

CHI-KUANG SUN, SHIH-WEI CHU, SHI-PENG TAI, STACIA KELLER,* A. ABARE,* U. K. MISHRA,* STEVEN P. DENBAARS*

Department of Electrical Engineering and Graduate Institute of Electro-Optical Engineering, National Taiwan University, Taipei, Taiwan, Republic of China; *Department of Electrical and Computer Engineering, University of California, Santa Barbara, California, USA

Summary: Taking advantage of the electric field-enhanced second-harmonic generation effect in bulk gallium nitride (GaN) and indium gallium nitride (InGaN) quantum wells, we demonstrated the piezoelectric field distribution mapping in bulk GaN and InGaN multiple-quantum-well (MQW) samples using scanning second-harmonic generation (SHG) microscopy. Scanning SHG microscopy and the accompanying third-harmonic generation (THG) microscopy of the bulk GaN sample were demonstrated using a femtosecond Cr:forsterite laser at a wavelength of 1230 nm. Taking advantage of the off-resonant electric field-enhanced SHG effect and the bandtail state-resonance THG effect, the second- and third-harmonic generation microscopic images obtained revealed the piezoelectric field and bandtail state distributions in a GaN sample. Combined with 720 nm wavelength excited two-photon fluorescence microscopy in the same sample, the increased defect density around the defect area was found to suppress bandedge photoluminescence, to increase yellow luminescence, to increase bandtail state density, and to decrease residue piezoelectric field intensity. Scanning SHG microscopy of the InGaN MQW sample was resonant excited with 800 nm femtosecond pulses from a Ti:sapphire laser in order to suppress SHG contribution from the bulk GaN substrate. Taking advantage of the strong piezoelectric field inside the InGaN quantum well, the wavelength resonant effect, and the electric field-enhanced SHG effect of InGaN quantum wells, resonant scanning SHG microscopy revealed the piezoelectric field distribution inside the wells. Combined with accompanying three-photon fluorescence microscopy from the bulk GaN substrate underneath the quantum wells, the direct correspondence between the piezoelectric field strength inside the quantum well and the substrate quality can be obtained. According to our study, the GaN substrate area with bright bandedge luminescence corresponds to the area with strong SHG signals indicating a higher stained-induced piezoelectric field. These scanning harmonic generation microscopies exhibit superior images of the piezoelectric field and defect state distributions in GaN and InGaN MQWs not available before. Combining with scanning multiphoton fluorescence microscopy, these techniques open new ways for the physical property study of this important material system and can provide interesting details that are not readily available by other microscopic techniques.

Key words: second harmonic generation, third harmonic generation, three-photon luminescence, electric field, gallium nitride

PACS: 42.65.Ky, 42.70.Nq, 71.55.Eq, 78.20.Hp

Introduction

Since the introduction of the scanning second-harmonic generation (SHG) microscopy technique by Gannaway and Sheppard in 1978, a scanning SHG microscope was used to obtain microscopic images of nonlinear materials including KD*P (Gannaway and Sheppard 1978), lithium niobate (Gannaway and Sheppard 1978), lithium triborate (Gauderon *et al.* 1998), and nonlinear poled polymers (Vydra and Eich 1998), as well as animal tissues (Freund *et al.* 1986; Guo 1996, 1997). Just like scanning two-photon fluorescence microscopy (Denk *et al.* 1990), scanning SHG microscopy can provide high axial/depth discrimination without a confocal aperture due to the quadratic dependence of the SHG signals on the laser intensity. Strong SHG signals are only induced in the vicinity of the focal point. The use of infrared wavelength leads to a greater penetration depth in most materials, providing the opportunity for imaging thicker samples. High-depth discrimination can be achieved with

Sponsored by the National Science Council, Taiwan, Republic of China, under grant number NSC 89-2112-M-002-082.

Address for reprints:

Chi-Kuang Sun
Dept. of Electrical Engineering and
Graduate Institute of Electro-Optical Engineering
National Taiwan University
Taipei, Taiwan
10617 Republic of China

optical sectioning with the soft aperture. Taking advantage of the nonlinear effect, harmonic generation can also avoid unnecessary out-of-focus bleaching and photo damages. Because of the nature of SHG, no absorption is needed in the generation process, which can even avoid focus damages and bleaching compared with multiphoton fluorescence microscopy. No staining of the specimen is required in SHG microscopy, which leads to more freedom in the choice of the experimental wavelength. However, the SHG nature also limits its application. It will not occur in centrosymmetric materials (Boyd 1992, Shen 1984). For the SHG process in surface or in noncentrosymmetric materials, the magnitude of the SHG signal depends on its specific phase-matching condition and the optical polarization, which makes the image interpretation difficult. The momentum conversation of the nonlinear process will make the reflection type measurement less desirable.

In this paper, we extend the SHG scanning microscopy to the mapping of electric field distribution, taking advantage of the electric field-induced SHG (EFISHG) effect, a third-order nonlinear response that generates an SHG signal intensity quadratically dependent on a dc electric field. The effect of EFISHG has been applied on the measurement of nonlinear susceptibility, in which the role of the electric field depends on the form of the sample. In the gas phase, an applied electric field breaks the symmetry of electronic states in atoms (Finn and Ward 1971) and molecules (Ward and Elliott 1978) and makes them second-harmonic active. In liquid solutions, EFISHG is employed to measure the second-order hyperpolarization of the molecule (Kishida *et al.* 1994). In solid, the electric field breaks the symmetry of the electronic state and makes SHG enhanced or possible (Terhune *et al.* 1962). The effect of EFISHG was even observed in a biological membrane where the electric field was modified by changing the voltage on the membrane (Bouevitch *et al.* 1993). In this paper we extend the EFISHG effect to scanning SHG microscopy for electric field mapping. We demonstrate the electric field mapping in bulk gallium nitride (GaN) and indium-gallium-nitride/gallium-nitride (InGaN/GaN) multiple quantum wells (MQWs) using scanning SHG microscopy with femtosecond optical pulses from a mode-locked Ti:sapphire laser or a modelocked Cr:forsterite laser. We have also performed scanning third-harmonic generation (THG) microscopy, scanning two-photon fluorescence microscopy, and scanning three-photon fluorescence microscopy of the GaN samples at the same time. Interesting information on the piezoelectric field distribution and its relation to the defect distribution, not available by other microscopy techniques, was obtained.

The recent demonstration of high brightness light-emitting diodes and laser diodes has established the III–V nitrides as key materials for optoelectronics operating in the green ultraviolet (UV) wavelength range (Nakamura and Fasol 1997; Nakamura 1998a, Nakamura *et al.* 1998b, 1999). Major developments of III–V nitride semiconductors have led to the commercial production of blue, green, and amber (Mukai *et al.* 1998, Nakamura 1998a, Nakamura *et al.* 1995) InGaN single-quantum-well light-emitting diodes and to the demonstration of InGaN MQW purple-blue laser diodes with lifetimes exceeding 10,000 h for continuous-wave (CW) operation at room temperature using nearly dislocation-free, overgrown GaN on sapphire (Nakamura *et al.* 1999) and GaN (Nakamura 1998a, Nakamura *et al.* 1998b) substrates. Although all practical devices contain InGaN in their active region, the emission mechanisms are not fully understood due to complex material physics and engineering of the InGaN alloy (Nakamura 1998a), such as phase separation (Behbehani *et al.* 1999) and piezoelectric field due to large lattice mismatch (Riblet *et al.* 1999, Schmidt *et al.* 1998b, Skromme *et al.* 1997, Wang *et al.* 1998). The optical behaviors of the GaN layer and the MQWs grown on top of the substrate layer were found to be strongly affected by high densities of defect states and large residue piezoelectric fields due to unrelaxed strain and instantaneous polarization (Riblet *et al.* 1999, Schmidt *et al.* 1998b, Skromme *et al.* 1997, Wang *et al.* 1998). Because of the large piezoelectric constants along the [0001] orientation in group III nitrides, built-in electric fields on the order of 1 MV/cm and 10–100 kV/cm are expected in InGaN/ GaN MQWs and bulk GaN films, respectively. Defect-related strong yellow luminescence and high density of bandtail states are frequently observed in most GaN materials. A considerable amount of studies has been devoted to clarify the roles of defect versus piezoelectric field in the photoluminescence spectra that are related to the laser mechanism. Several groups (Chichibu *et al.* 1997, Schmidt *et al.* 1998a) have assigned the spontaneous emission from InGaN quantum wells to the recombination of excitons localized at certain potential minimum in bandtail states. On the other hand, several groups have discussed the importance of the quantum-confined Stark effect (QCSE) due to the piezoelectric field in strained wurzite InGaN QWs (Riblet *et al.* 1999, Takeuchi *et al.* 1997, Wang *et al.* 1998). The blue shift of the electroluminescence peak in InGaN QWs with an increasing drive current has been explained by the combined effects of a reduction in QCSE (Wang *et al.* 1998) due to space-charge screening and bandfilling of the bandtail states (Chichibu *et al.* 1997, Schmidt *et al.* 1998b). To obtain more detailed insight into the dominant emission properties of the bulk GaN substrate and the InGaN QWs grown on top of the bulk GaN substrate, it is essential to develop a microscopic tool for investigation of the relative effects and distributions of the defect-related bandtail states and the strain-induced piezoelectric field.

Recently, Miragliotta and Wickenden (1996) reported on the observation of strong electric field-induced second-harmonic generation in bulk GaN. With a wurzite structure and a 6 mm group symmetry, GaN is a uniaxial crys-

tal with the effective second order susceptibility $\chi^{(2)}$ expressed as (Miragliotta and Wickenden 1996)

$$\chi_{ijk}^{(2)eff}(2\omega:\omega,\omega) = \chi_{ijk}^{(2)}(2\omega:\omega,\omega) + 3\chi_{ijkl}^{(3)}(2\omega:\omega,\omega,0)E_l \quad (1)$$

where the second term in Eq. (1) represents the EFISHG effect with E_l as the strength of the DC electric field. By applying a large DC electric field to the surface of a GaN film, Miragliotta and Wickenden (1996) have reported a value of 1.3×10^{-11} m/V for $\chi_{zxx}^{(2)}(2\omega:\omega,\omega)$ and a value of 5.3×10^{-19} m^2/V^2 for $\chi_{zxxz}^{(3)}(2\omega:\omega,\omega,0)$ at a wavelength around the midgap of GaN (1.71 eV). According to their study, a positive electric field on the order of 10 kV/cm can increase 10% value of the effective $\chi^{(2)}$ and 20% value of the generated SHG power. This strong EFISHG effect can be attributed to the large $\chi^{(3)}$ process in GaN. Recent studies of the $\chi^{(3)}$ process in GaN indicated strong third-order nonlinearities in GaN materials, including nonlinear refractive index (Huang *et al.* 1999), two photon absorption (Sun 2000b), and third harmonic generations (Miragliotta and Wickenden 1994). Miragliotta and Wickenden (1994) have experimentally determined the third-order susceptibility $\chi_{xxxx}^{(3)}(3\omega:\omega,\omega,\omega)$ in bulk GaN to be on the order of 3.8×10^{-19} m^2/V^2 at a wavelength one third of the bandgap energy (1.13 eV). For MQW structures, taking into account the strain-induced piezoelectric field, piezoelectric field-enhanced, second-order nonlinear optical susceptibility was also reported in wurzite GaN/AlGaN quantum wells (Liu *et al.* 2000). Strong $\chi^{(2)}$, which was an order of magnitude larger than the bulk value, was observed in InGaN/GaN quantum wells (Schmidt *et al.* 1999). By scanning the SHG power after the bulk GaN samples and the InGaN MQW samples, we are thus able to map the residue piezoelectric field distribution in the GaN-based samples.

Materials and Methods

The experiments were performed on a bulk GaN Hall measurement thin-film sample and an InGaN/GaN MQW sample. The bulk GaN thin film was grown by metal organic chemical vapor deposition (MOCVD) on c-plane sapphire in an atmospheric pressure reactor. After annealing the substrate at 1050°C, a 52.5 nm thick nucleation layer was deposited at 600°C (Keller *et al.* 1995). The temperature was then raised to 1080°C to grow an unintentionally doped GaN layer of 2.5 μm thickness. The n-type carrier concentration on the bulk GaN layer was ~5×10^{16} cm^{-3}. The crystal structure was wurzite (Keller *et al.* 1995). The corresponding photoluminescence (PL) spectrum excited by a CW HeCd laser is shown in Figure 1. Strong bandgap luminescence at 365 nm (3.39 eV) can be observed. Below the bandgap luminescence, a weak bandtail luminescence between 365 and 390 nm and a weak yellow luminescence centered at 550 nm can be observed. Similar results were widely observed in most unintentional doped GaN samples (Qui *et al.* 1995). Regarding the formation of these extended bandtail states, some previously explored mechanisms might be responsible, including local stresses (Sturge 1962), perturbations of the band structure by Coulomb potential of ionized impurities (Redfield and Aframowitz 1967), and high density of defect states (Kane 1963).

For the MQW sample, MQWs with 14 periods of undoped InGaN wells with 1.2 nm well width and 4.3 nm thick GaN:Si barriers were grown on top of a 2.5 μm thick unintentionally doped GaN substrate. The indium content is 10%. The structure was finished with a 100 nm thick AlGaN cap layer with 6% Al content. Detailed optical properties of the MQW sample were published in a previous paper (Chichibu *et al.* 1999) and a piezoelectric field on the order of 0.5 MV/cm was derived inside the quantum well. The PL measurement of the MQW sample showed a luminescence peak around 3.11 eV (Chichibu *et al.* 1999), which was influenced by and red-shifted due to bandtail defect states. The absorption spectrum of the MQW sample is shown in Figure 2. According to this figure, the bandgap energy of the 1.2 nm InGaN MQW is located around 395 nm (3.14 eV). The sharp rise of the absorption at 365 nm is attributed to the absorption in the GaN substrate underneath.

The experiments were performed using either a femtosecond Ti:sapphire laser or a femtosecond Cr:forsterite laser. The Kerr-lens-modelocked Ti:sapphire laser (Model: Tsunami, Spectra-Physics Inc., Mountain View, Calif., USA) was pumped by a 5 W CW frequency-doubled Nd:YVO_4 laser (Model: Millennia, Spectra-Physics Inc, Mountain View, Calif., USA) with 500 mW average output power. It generates 150 femtosecond optical pulses with a repetition rate of 80 MHz. The laser output wavelength was tunable between 690 and 810 nm. By chang-

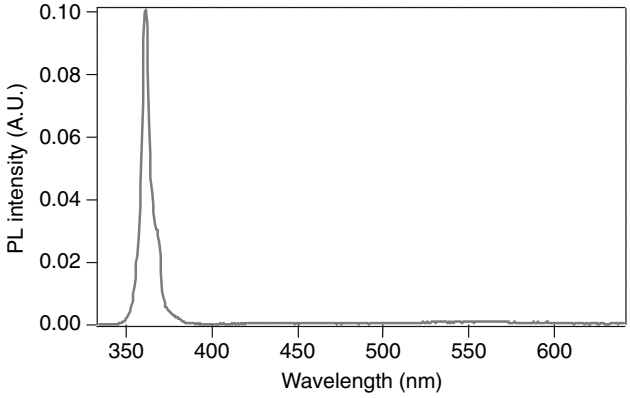

FIG. 1 Photoluminescence (PL) spectrum of a bulk GaN sample excited by a continuous-wave (CW) HeCd laser. Luminescence peak at 365 nm (3.39 eV) corresponds to bandedge emission. Below the bandgap luminescence, a weak bandtail luminescence between 365 and 390 nm and a weak yellow luminescence centered at 550 nm can be observed. A.U. = arbitrary unit.

ing mirror sets, this femtosecond Ti:sapphire laser output wavelength can be extended to 980 nm.

The home-built Cr:forsterite laser constructed for this study uses a 19 mm long Brewster-cut Cr^{4+}:forsterite crystal with its b-axis on the horizontal plane, resulting in horizontal polarization for the lasing fundamental beam. The crystal temperature was kept around 2°C. The laser was pumped with an 8W of 1064 nm light from a diode-pumped Nd:YVO_4 laser (Model: Millennia IR, Spectra-Physics Inc.) At the output of the pump laser, a pump lens was placed to adjust the size of the pumping laser beam. After turning polarization of the pumping beam by a periscope, it was focused with a 10 cm lens through a high-reflecting cavity mirror onto the Cr^{4+}: forsterite crystal. The laser cavity was a Z-cavity consisting of a 4.5% output coupler and a semiconductor saturable absorber mirror (SESAM). For confocal microscopy, the employment of the SESAM will initiate and stabilize the femtosecond pulse generation even with back reflection from the external cavity. In our study, the SESAM consisted of 25 periods of GaAs/AlAs quarter wave layers, followed by an $Al_{0.48}In_{0.52}As$ quarter wave layer with two embedded $Ga_{0.47}In_{0.53}As$ quantum wells. To provide the saturable absorber nonlinearity for initiating and stabilizing the Cr^{4+}:forsterite laser, the quantum-well structure was designed to have the heavy-hole excitonic resonance at 1232 nm at room temperature. The insertion loss of the SESAM is 2.5% with a saturation energy ~50 μJ/cm^2. An SF6 prism pair was inserted to provide intracavity group-velocity dispersion compensation. Before the output coupler, a slit was used to tune the fundamental wavelength. Outside the cavity, we used another SF6 prism pair to achieve both beam shaping and dispersion compensation of the fundamental output. The output wavelength was centered at 1230 nm with a pulsewidth of 150 femtoseconds. The maximum average output power was around 350 mW with 125 MHz repetition rate. Without the SESAM, the output wavelength can be extended to 1270 nm, which was limited by our mirror coating and the output coupler coating.

Figure 3 shows the experimental setup. The femtosecond infrared (IR) laser beam was shaped by a telescope and then focused into a GaN sample with an 80× IR applicable objective (Model: ULWD MIR 80×, Olympus Optical Co., Ltd, Tokyo, Japan) with numerical aperture (NA)=0.75. The focused spot size was approximately 1.3 μm. The generated harmonic generation and multiphoton fluorescence signals were collected and collimated using an opposing objective. We filtered out the fundamental IR beam with an optical glass filter. The collected red/purple light was then directed into a spectrometer (Model: Cornerstone 130, Oriel Instruments, Stratford, Conn., USA) for the spectrum measurements. Due to the relatively large harmonic generation signals, an umamplified Si photodetector (Model DET100, Thorlab Inc, Newton, N.J., USA) will be suitable for the light detection. Second-harmonic generation, third-harmonic generation-, two-photon absorption-, and three-photon absorption-induced PL can all be observed in the spectrum. Their corresponding scanning images can then be obtained by moving the GaN sample in the plane (called "x-y" plane) perpendicular to the sample c-axis (extraordinary axis, or z-axis) by using XYZ 0.1 μm stepping motor-driven stages (Model: UTM50PP.1, Newport Corp., Irvine, Calif., USA).

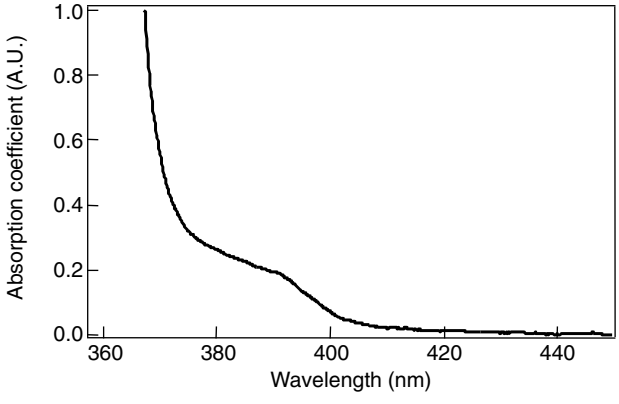

FIG. 2 Absorption spectrum of an InGaN multiple quantum well (MQW) sample with 1.2 nm wellwidth. The rise of the absorption of approximately 395 nm (3.14 eV) corresponds to the MQW bandgap transition energy. The sharp rise of the absorption at 365 nm is due to the absorption in the GaN substrate underneath. A.U. = arbitrary unit.

Results and Discussions

Bulk GaN Sample

The experiment was first performed in the bulk GaN sample. Even though it seems straightforward to use a femtosecond Ti:sapphire laser that can provide the necessary short pulses and the bandgap resonant second-harmonic wavelength to perform the electric field mapping in the bulk GaN sample, the close resonance wave-

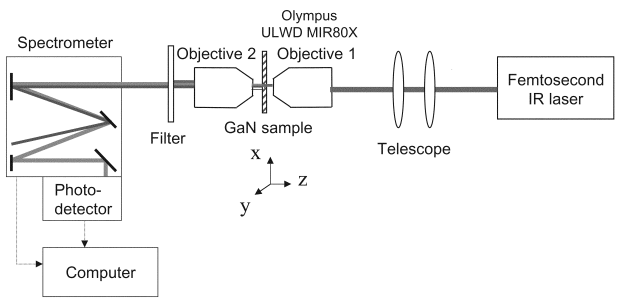

FIG. 3 Experimental layout for the scanning second- and third- harmonic generation (SHG/THG) microscopy of GaN. IR = infrared.

length will also make the generated SHG power sensitive to the distribution of the defect-related bandtail states in the sample. This effect will seriously influence the interpretation of the SHG scanning images, especially for the bulk GaN substrate that has a weaker residue electric field. In this case, the scanning SHG image will not be able to separate the effects of the piezoelectric field from defect distribution and the obtained SHG images will be hard to interpret. One way to solve this problem is to move the laser wavelength away from the resonance. In our study, we performed the scanning SHG microscopy of bulk GaN using the femtosecond Cr:forsterite laser with a wavelength of 1230 nm, which is off resonance from the GaN bandgap. By using a wavelength of approximately 1230 nm we cannot only use off-resonant SHG intensity to map the piezoelectric field distribution, but we can also obtain close resonance THG signals, which would be enhanced by the bandtail states. This bandtail state-enhanced THG image can then be used to probe the distribution of defect-related bandtail states, whose role versus the piezoelectric field on the photoluminescence of GaN based devices has long been discussed and debated.

After focusing the 1230 nm femtosecond light onto the bulk GaN sample, visible red and purple light corresponding to the SHG and THG signals generated from the GaN sample can be easily observed. Figure 4 shows some typically measured SHG/THG spectra. The laser spectrum is also provided for comparison. With a fundamental wavelength centered on 1230 nm, symmetric SHG/THG spectra centered on 615 and 410 nm can be observed. For the SHG/THG applications in GaN imaging, there are several problems we have to consider. Due to the fact that most GaN samples are grown in the direction of c-axis, a scanning in the plane perpendicular to the sample c-axis would be preferred. However, there are only 7 $\chi^{(2)}$ components existing in wurzite structures (xzx=yzy, xxz=yyz, zxx=zyy, and zzz) (Shen 1984). To generate SHG in GaN, an angle between beam propagation direction and the c (z)-axis is required. To map out the EFISHG signal induced by a piezoelectric field in z direction, a similar requirement will be necessary. This SHG requirement obviously violates the preferred scanning arrangement that requires a zero degree angle between the beam propagation direction and the sample c-axis. The problem was solved by using a tightly focused laser beam with the 80× objective, which would induce curved wavefronts around the focal point and provide the required optical-field z components. To make the curved wavefront fall side the thin sample, the sample thickness should be on the order of the confocal parameter of the focused laser beam, which was our case with the 80× objective. Figure 5 shows the angle-dependent SHG power on the GaN sample with an 80× and a 50× objective. As shown in Figure 5, weaker angle dependence of SHG can be achieved when we focused the laser beam with a higher NA objective. Excellent SHG power can be observed at 0 incident angle using the 80× objective in the 2.5 μm thick GaN sample. Another advantage of using longer IR wavelength to perform the SHG image in GaN is the increase of the SHG coherent length due to lower refractive index dispersion in the longer wavelength region (Kawashima *et al.* 1997, Yu *et al.* 1997, Zhang *et al.* 1996). The calculated coherent length of the SHG process using the 1230 nm IR wavelength is approximately 10 μm, which is much longer than our sample thickness and ensures efficient SHG process in our experimental arrangement.

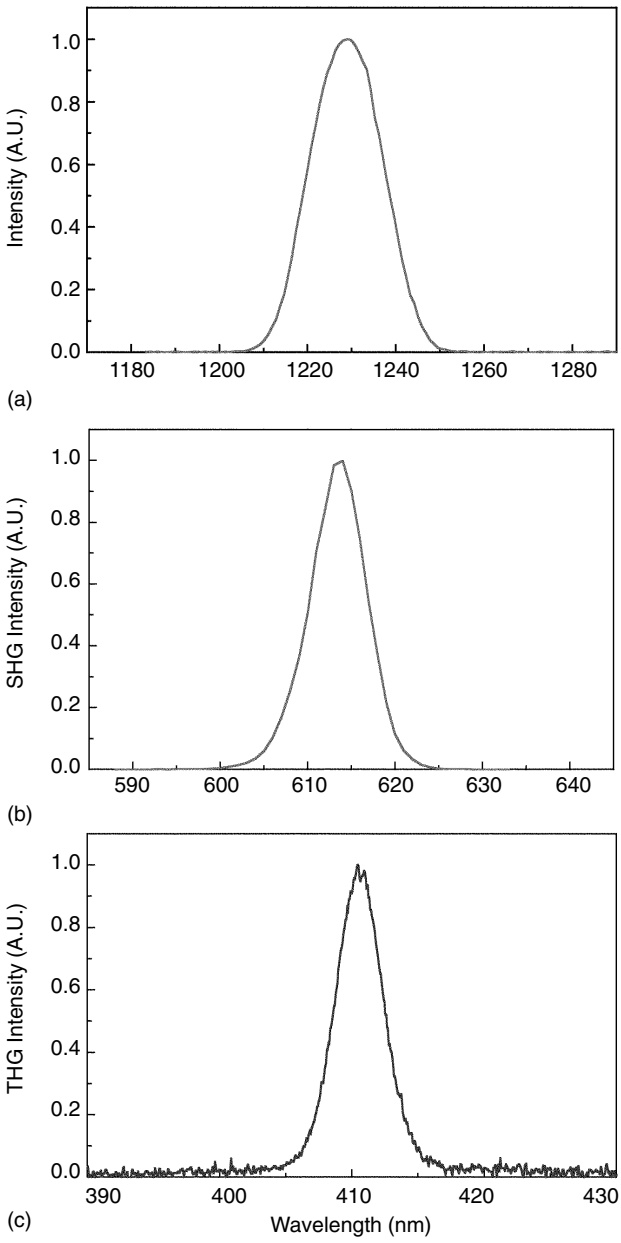

FIG. 4 Spectra for (a) infrared (IR) laser beam, (b) second-harmonic generation (SHG), and (c) third-harmonic generation (THG) signals from a 2.5 μm-thick bulk GaN. The IR laser output from a femtosecond Cr:forsterite laser was centered at 1230 nm, while the SHG and THG spectra are centered at 615 nm and 410 nm respectively. A.U. = arbitrary unit.

For THG microscopy, the $\chi^{(3)}_{xxxx}$ component will provide the necessary THG process for a laser beam with x-polarized light. However, the positive dispersion in GaN will limit the effective THG generation only in the surface layer thinner than the confocal parameter (Boyd 1992). The large refractive index difference (Kawashima *et al.* 1997, Yu *et al.* 1997, Zhang *et al.* 1996) between the fundamental IR (1230 nm) and the THG purple light (410 nm) would also limit the coherent length of the THG process to be on the order of only 1 μm. The latter process will reduce the THG signals from a thicker sample for the already weak third-order process. This situation was improved in our experiments because of the close resonant excitation scheme.

Figures 6 and 7 show the measured SHG and THG average power versus input IR average power for the 2.5 μm thick bulk GaN sample by using the 80× objective with laser beam propagating in the c-axis (0 incident angle). With a 45 mW input power, an SHG output power of 140 nW and a THG output power of 10 nW can be obtained. Open circles are the experimental data and the dashed lines correspond to square dependence and cubic dependence of the output-input relations for Figures 6 and 7, respectively. Slopes of 2 and 3 can be found in the log-log plots confirming the SHG and THG origins of the measured signals. A value of 3×10^{-12} m/V for $\chi^{(2)}_{eff}(2\omega{:}\omega,\omega)$ and a value of 1×10^{-20} m^2/V^2 for $\chi^{(3)}_{xxxx}(3\omega{:}\omega,\omega,\omega)$ can thus be derived from our data for our specific experimental wavelengths.

With efficient SHG and THG powers, SHG and THG scanning microscopic images can thus be easily obtained by scanning the sample in the XY plane perpendicular to both the sample growth and beam propagation directions. Figure 8 shows the scanning SHG microscopic image and its corresponding scanning THG microscopic image of the GaN bulk Hall-measurement sample (paradermal view). A transmission image taken with the fundamental IR beam is also presented for comparison. The image was taken from the edge of the Hall-measurement sample with an oval defect. The GaN sample shows excellent lateral uniformity in the SHG generation, except in the area around the oval defect, where decreased SHG intensity can be observed. It is interesting to notice that the heart-shaped area generating weak SHG signals around the oval defect emitted strong THG signals. Figure 9 shows a line scan of the SHG intensity and its corresponding THG intensity across the oval defect. The position of the performed line scan is shown in the inset of Figure 9. The SHG and THG powers are normalized for comparison. Opposite trends of the SHG and THG intensities can be observed. Enhanced THG signals can be seen around the oval defect where suppressed SHG signals were observed.

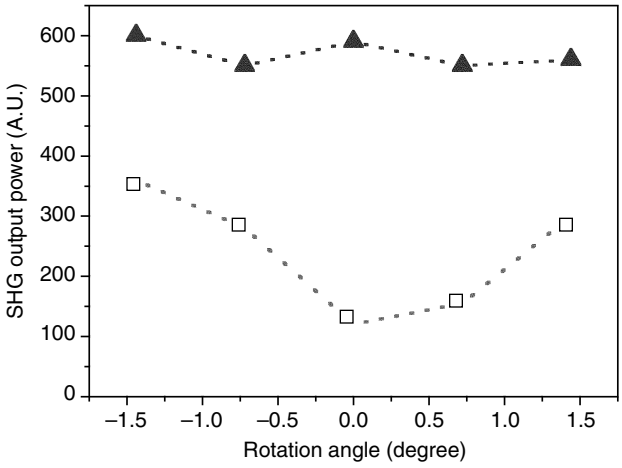

FIG. 5 Angle-dependent second-harmonic generation (SHG) powers on the bulk GaN sample with an 80× and a 50× objective.

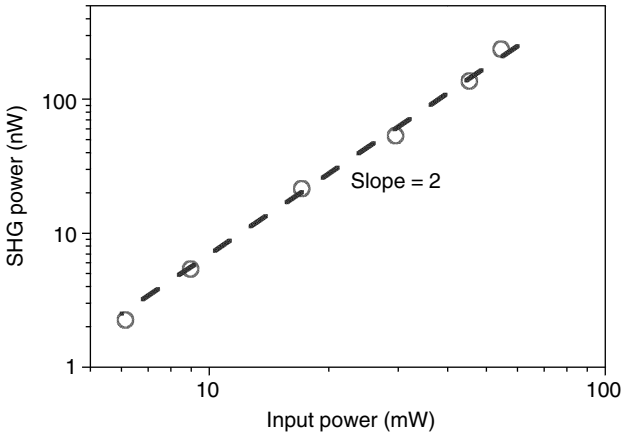

FIG. 6 Average second-harmonic generation (SHG) power versus average input infrared power in a 2.5 μm thick GaN sample. The experiment was performed with an 80× objective. The open circles are experimental data and the dashed line is a guided line with a slope of 2.

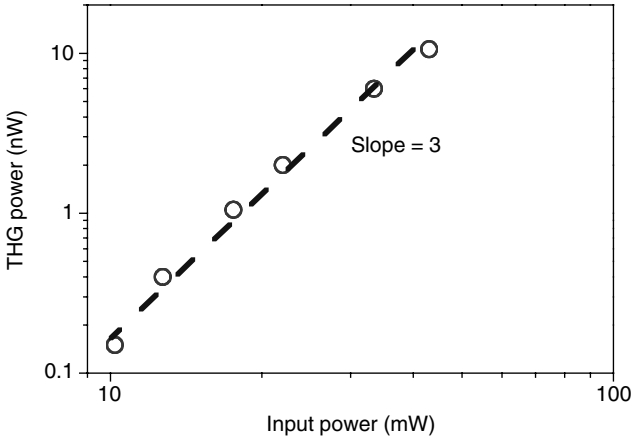

FIG. 7 Average third-harmonic generation (THG) power versus average input infrared power in a 2.5 μm thick GaN sample. The experiment was performed with an 80× objective. The open circles are experimental data and the dashed line is a guided line with a slope of 3.

The sharp decrease of the signals at the edge of the oval defect is due to the unflat sample surface around the edge, which caused the SHG/THG signals to be misaligned with the detection system due to a sample lensing effect. Our data suggest that in the heart-shaped area around the oval defect, the THG signals were resonantly enhanced due to increased bandtail state densities that were reflected by the measured THG signals. At the same time, these defects reduced the residue piezoelectric field by strain relaxation or by a space charge screening effect, resulting in decreased SHG signals in the same area due to the decreased EFISHG effect.

We can also perform three-dimensional mapping of the SHG and THG images by moving the stage in the XYZ directions. Figures 10 and 11 show the x-z, y-z, as well as the x-y directional scans of the sample SHG and THG signals. The white lines on top of the x-y images indicate the positions of the z-directional scans. Better z-direction resolution in the scanned THG image can be observed, compared with that of the SHG image due to its cubic power dependence and short coherent length. As shown in Figures 10 and 11, the z-direction resolution is strongly limited by the thin sample thickness. Post-data-processing using a deconvolution program would be necessary to improve the z-direction resolution.

It is also interesting to compare the scanning SHG/THG microscopy with other scanning multiphoton fluorescence microscopies. We have previously performed two-photon fluorescence microscopy in the same Hall measurement sample by using 720 nm wavelength femto-

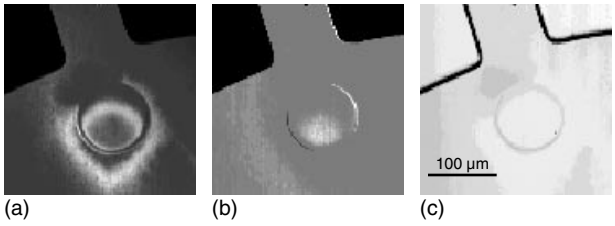

FIG. 8 (a) Scanning third-harmonic generation image, (b) scanning second-harmonic generation image, and (c) their corresponding transmission image of a GaN Hall-measurement sample. The transmission image was taken with the fundamental infrared beam.

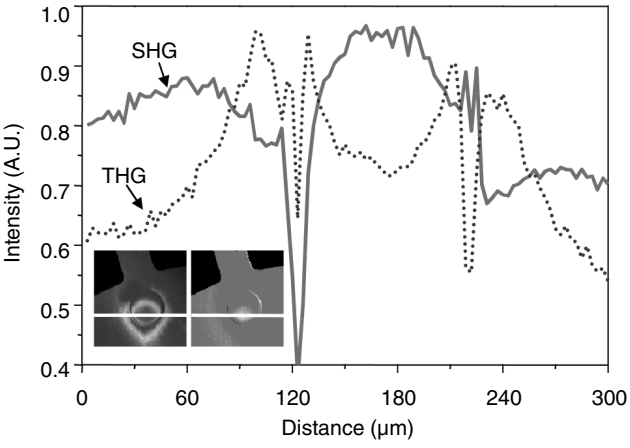

FIG. 9 Linescan of the second-harmonic generation intensity and its corresponding third-harmonic generation intensity across the oval defect in a GaN sample. The position of the performed linescan is shown in the inset. A.U. = arbitrary unit.

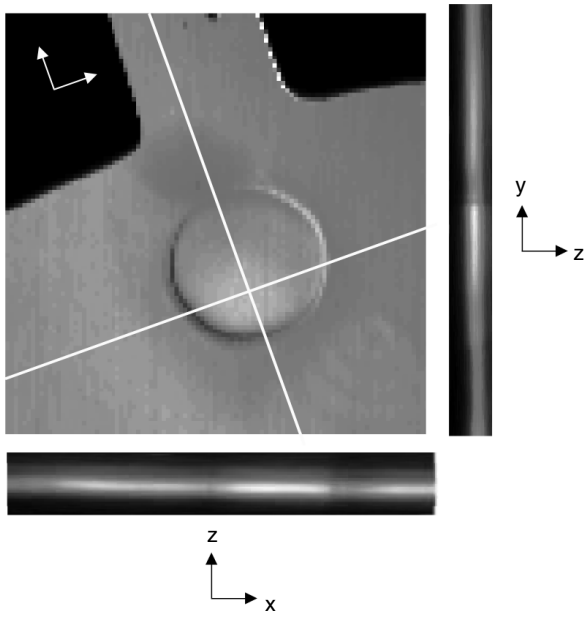

FIG. 10 x-z, y-z, and their corresponding x-y scanned second-harmonic generation images of the bulk GaN sample. The white lines on top of the x-y image indicate the positions of the z-directional scans.

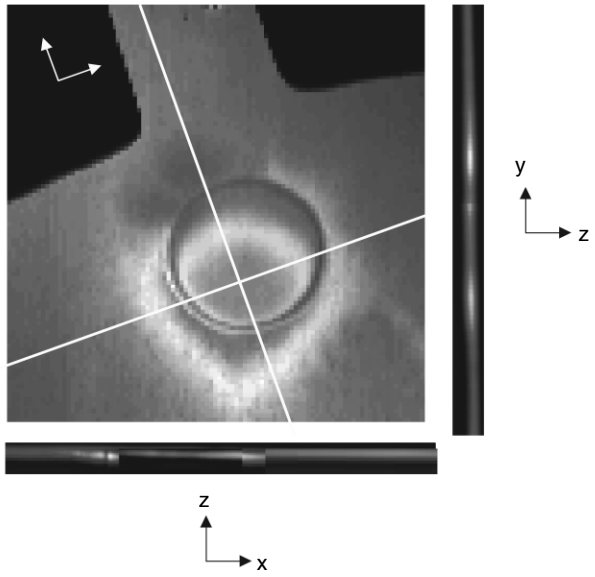

FIG. 11 x-z, y-z, and their corresponding x-y scanned third-harmonic generation images of the bulk GaN sample. The white lines on top of the x-y image indicate the positions of the z-directional scans.

second pulses generated from the Ti:sapphire laser (Sun *et al.* 2000b). Excellent two-photon fluorescence images taken at both bandedge-luminescence wavelength and yellow-luminescence wavelength around the oval defect were obtained. As shown in Figure 4 of our previously published paper (Sun *et al.* 2000b), the two-photon fluorescence images indicated that the heart-shaped area generating strong THG signals around the oval defect emitted strong yellow luminescence with strongly suppressed bandedge PL. Our microscopy studies thus indicate the connections between suppressed bandedge PL, increased yellow luminescence, increased bandtail state density, and decreased residue piezoelectric field due to increased defect densities around the defect in a bulk GaN sample.

InGaN Multiple Quantum Well Sample

We have also extended our piezoelectric field mapping to the MQW sample. The piezoelectric field in InGaN quantum wells strongly modifies their optical and electrical behaviors through quantum-confined Stark effect (Im *et al.* 1998, Riblet *et al.* 1999, Takeuchi *et al.* 1997, Wang *et al.* 1998) and quantum-confined Franz-Keldysh effect (Chichibu *et al. 1998*, Sun *et al.* 2000a). The piezoelectric field inside the quantum wells separated the electron and hole wavefunctions and caused the observed nonambipolar carrier diffusion (Huang *et al.* 2001) and the observed long carrier recombination lifetime (Minsky *et al.* 1998). The huge piezoelectric field inside InGaN MQW was also responsible for the observed strong coherent acoustic phonon oscillation (Sun *et al.* 2000a). The strain-induced piezoelectric field in InGaN MQWs depends strongly on the quality and the strain of the GaN substrate underneath the MQWs. To understand the piezoelectric field uniformity and its relation with the substrate quality, it is essential to perform microscopic piezoelectric field mapping so as to understand the detailed physical mechanisms.

We have performed the SHG mapping using the femtosecond Cr:forsterite laser in the MQW sample. However, the SHG signals from the MQWs will be mixed with the SHG signals from the GaN substrate, which makes the SHG microscopic image hard to understand. With an excitation wavelength of 1230 nm, the relative contribution of the SHG signals from the GaN substrate and the MQW is on the order of 5:1, and the SHG signal strength was found to be independent of the well width. To obtain only the piezoelectric field information inside the InGaN MQWs, we excited the SHG in the MQW using resonant IR wavelength. According to previous studies performed by Schmidt *et al.* (1999), resonant excitation with the two-photon wavelength close to but slightly below the QW fundamental transition will avoid two-photon absorption and enhance the SHG in MQW. Thus obtained SHG under this situation will be symmetric in spectrum and will be dominated by the SHG from MQWs as shown in Figure 2 in the paper by Schmidt *et al.* (1999).

With a bandgap transition wavelength of 395 nm, we performed the piezoelectric field mapping inside the InGaN MQW using 800 nm femtosecond pulses from the Ti:sapphire laser by mapping the resonant enhanced SHG signals in the xy plane perpendicular to the sample growth direction (c-axis). According to Liu *et al.* (2000), the large piezoelectric field in the wurzite InGaN quantum wells beaks the symmetry of the confinement potential profile and leads to large second-order nonlinear optical susceptibilities. The magnitude of this electric field-enhanced SHG signal should thus reflect the strength of the piezoelectric field inside the quantum wells. Figure 12 shows the fundamental IR spectrum of the Ti:sapphire and the obtained SHG spectrum after the MQW sample. With a symmetric IR spectrum centered at a wavelength of 800 nm, the obtained nonlinear spectrum was centered at 400 nm also with a symmetric spectral shape, reflecting the nature of SHG. It is interesting to notice that the luminescence peak centered at 365 nm was also observed in the nonlinear spectrum, which is due to three-photon

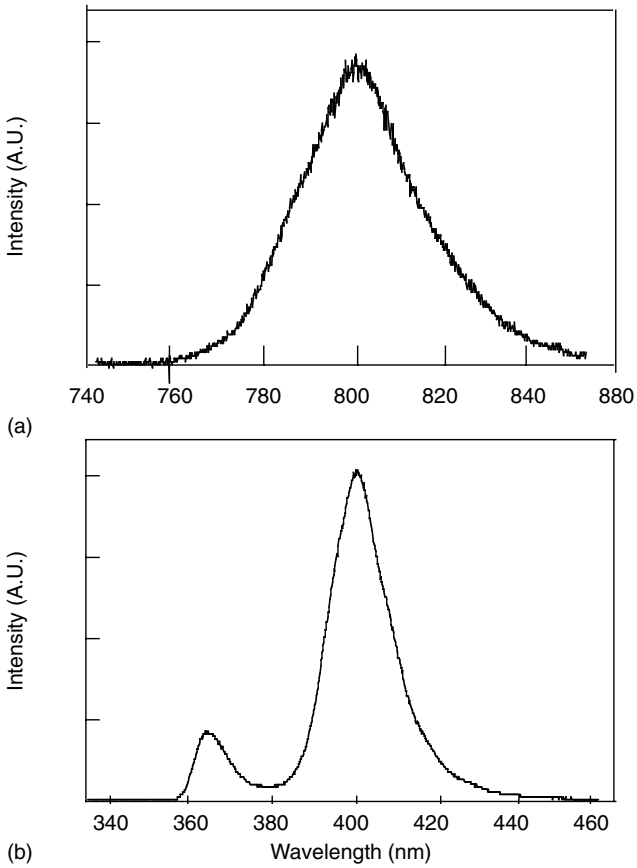

FIG. 12 (a) Fundamental infrared spectrum of the Ti:sapphire centered at 800 nm and (b) the excited nonlinear spectrum after the InGaN multiple quantum well sample. The symmetric spectrum centered at 400 nm is the generated second-harmonic generation. The luminescence peak centered at 365 nm corresponds to the three photon-induced bandedge photoluminescence from the GaN substrate. A.U. = arbitrary unit.

absorption-induced bandgap luminescence from the bulk GaN substrate underneath the MQW structures. The observed optical behaviors and the power dependence of the SHG signals in InGaN MQWs and three-photon absorption-induced bandgap luminescence in the bulk GaN substrate were similar to those of previous studies by Schmidt *et al.* (1999) and Kim *et al.* (1997).

Figure 13 shows the scanning SHG microscopic image and its corresponding scanning three-photon bandgap luminescence microscopic image of the InGaN MQW sample (paradermal view) obtained by scanning the sample in the xy plane perpendicular to both the sample growth and beam propagation directions. With a resonant excitation wavelength of 800 nm, the observed SHG image (taken at 400 nm) reflects the piezoelectric field distribution inside the InGaN MQW, and the obtained three-photon bandgap luminescence image (taken at 365 nm) reflects the quality of the GaN substrate, which is similar to the two-photon bandgap luminescence image of the bulk GaN sample described in the previous subsection. With the MQW structures facing the laser source, the absorption of the 365 nm bandgap luminescence by the InGaN MQW before our detection can be avoided. The observed three-photon bandgap luminescence should thus directly reflect the GaN substrate quality. We observed uniform SHG images from most areas of the MQW sample. Figure 13a shows the SHG image (taken at 400 nm) in a region with a bright donut-type area, indicating strong piezoelectric field distribution in this donut-shaped area. We have also observed dark SHG spots, probably due to weak local fields. The corresponding three-photon bandgap PL mapping in Figure 13b taken at 365 nm shows a similar image with the same bright donut-type area, reflecting the high substrate quality in this bright area. Similar correspondence can also be seen for dark spots, indicating the direct correspondence between the GaN substrate quality and the piezoeletric field strength inside the InGaN MQWs grown on top of it. This is probably related to the strain relaxation inside InGaN MQW due to defects like dislocations in the GaN substrate. Our developed techniques in bulk GaN and InGaN nonlinear imaging obviously provide fruitful information on the relation between the piezoelectric field and defects in the MQW and their corresponding GaN substrate. These nonlinear spectroscopic microscopies in bulk GaN and MQW structures, including SHG, THG, two-photon PL, and three-photon PL, open new ways for the studies of this important material system and can provide information not available from any other microscopic technique before.

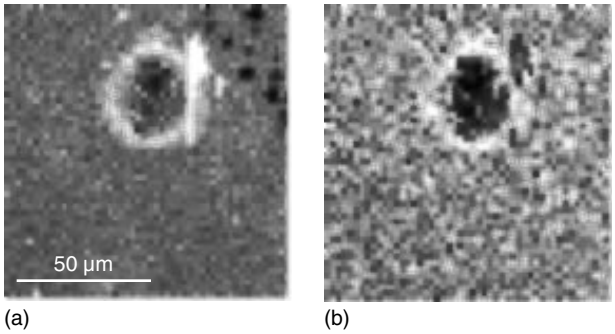

FIG. 13 (a) Scanning second-harmonic generation (from InGaN multiple quantum well [MQW]) image and (b) its corresponding scanning three-photon bandgap luminescence (from GaN substrate) image of the InGaN MQW sample (paradermal view).

Conclusion

Taking advantage of the electric field-enhanced SHG effect in bulk GaN and InGaN quantum wells, we demonstrated the piezoelectric field distribution mapping in a bulk GaN sample and in InGaN multiple-quantum-well samples using scanning SHG microscopy. Scanning SHG microscopy and the accompanying THG microscopy of the bulk GaN sample were demonstrated using a femtosecond Cr:forsterite laser at a wavelength of 1230 nm. Taking advantage of the off-resonant electric field-enhanced SHG effect and the bandtail-state resonance THG effect, the obtained SHG and THG microscopic images revealed the piezoelectric field and bandtail state distributions in the GaN sample. Combined with a 720 nm wavelength excited two-photon fluorescence microscopy in the same sample, the increased defect density around the defect area was found to suppress bandedge photoluminescence, to increase yellow luminescence, to increase bandtail state density, and to decrease residue piezoelectric field intensity. Scanning SHG microscopy of the InGaN MQW sample was resonant excited with 800 nm femtosecond pulses from a Ti:sapphire laser in order to suppress SHG contribution from the bulk GaN substrate. Taking advantage of the strong piezoelectric field inside the InGaN quantum well, the wavelength resonant effect, and the electric field-enhanced SHG effect of InGaN quantum wells, the resonant scanning SHG microscopy revealed the piezoelectric field distribution inside the wells. Combined with the accompanied three-photon fluorescence microscopy from the bulk GaN substrate underneath the quantum wells, the direct correspondence between the piezoelectric field strength inside the quantum well and the substrate quality can be obtained. According to our study, the GaN substrate area with bright bandedge luminescence corresponds to the area with strong SHG signals, indicating a higher stain-induced piezoelectric field. These SHG microscopies exhibit superior images of the piezoelectric field and defect state distributions in GaN and InGaN MQWs not available previously. In combination with scanning multiphoton fluorescence microscopy, these techniques open new ways to the physical property studies of this important material system and can provide interesting details that are not readily available by other microscopic techniques.

Acknowledgment

The authors would like to acknowledge the stimulating scientific discussions with H. Schmidt and A. Imamoglu.

References

Behbehani MK, Piner EL, Liu SX, El-Marsy NA, Bedair SM: Phase separation and ordering coexisting in InGaN grown by metal organic chemical vapor deposition. *Appl Phys Lett* 75, 2202–2204 (1999)

Bouevitch O, Lewis A, Pinevsky I, Wuskell JP, Loew LM: Probing membrane potential with nonlinear optics. *Biophys J* 65, 672–679 (1993)

Boyd RW: *Nonlinear Optics*. Academic Press, San Diego (1992)

Chichibu S, Abare AC, Mack MC, Minsky MS, Deguchi T, Cohen D, Kozodoy P, Fleischer SB, Keller S, Speck JS, Bowers JE, Hu E, Mishra UK, Coldren LA, DenBaars SP, Wada K, Sota T, Nakamura S: Optical properties of InGaN quantum wells. *Mater Sci Eng* B59, 298–306 (1999)

Chichibu S, Abare AC, Minsky MS, Keller S, Fleischer SB, Bowers JE, Hu E, Mishra UK, Coldren LA, DenBaars SP: Effective bandgap inhomogeneity and piezoelectric field in InGaN/GaN multiquantum well structures. *Appl Phys Lett 73*, 2006–2008 (1998)

Chichibu S, Azuhata T, Sota T, Nakamura S: Luminescence from localized states in InGaN epilayers. *Appl Phys Lett* 70, 2822–2824 (1997)

Denk W, Strickler JH, Webb WW: Two-photon laser scanning fluorescence microscopy. *Science* 248, 73–76 (1990)

Finn RS, Ward JF: Dc-induced optical second harmonic generation in the inert gases. *Phys Rev Lett* 6, 285–289 (1971)

Freund I, Deutsch M, Sprecher A: Connective tissue polarity: Optical second-harmonic microscopy, crossed-beam summation, and small-angle scattering in rat-tail tendon. *Biophys J* 50, 693–712 (1986)

Gannaway JN, Sheppard CJR: Second-harmonic imaging in the scanning optical microscope. *Opt Quantum Electron* 10, 435–439 (1978)

Gauderon R, Lukins PB, Sheppard CJR: Three-dimensional second-harmonic generation imaging with femtosecond laser pulses. *Opt Lett* 23, 1209–1211 (1998)

Guo Y, Ho PP, Savage H, Harris D, Sacks P, Schantz S, Liu F, Zhadin N, Alfano RR: Second-harmonic tomography of tissues. *Opt Lett* 22, 1323–1325 (1997)

Guo Y, Ho PP, Tirksliunas A, Liu F, Alfano RR: Optical harmonic generation from animal tissues by the use of picosecond and femtosecond laser pulses. *Appl Opt* 22, 6810–6813 (1996)

Huang Y-C, Liang J-C, Sun C-K, Abare A, DenBaars SP: Piezoelectric-field enhanced lateral ambipolar diffusion coefficient in InGaN/GaN multiple quantum wells. *Appl Phys Lett* 78, 928–930 (2001).

Huang Y-L, Sun C-K, Liang J-C, Keller S, Mack MP, Mishra UK, DenBaars SP: Femtosecond Z-scan measurement of GaN. *Appl Phys Lett* 75, 3524–3526 (1999)

Im J, Kollmer H, Off J, Sohmer A, Scholz F, Hangleiter A: Reduction of oscillator strength due to piezoelectric fields in InGaN/AlGaN quantum wells. *Phys Rev* B 57, 9435–9438 (1998)

Kane EO: Thomas-Fermi approach to impure semiconductor band structure. *Phys Rev* 131, 79–88 (1963)

Kawashima T, Yoshikawa H, Adachi S, Fuke S, Ohtsuka K: Optical properties of hexagonal GaN. *J Appl Phys* 82, 3528–3535 (1997)

Keller BP, Keller S, Kapolnek D, Jiang W-N, Wu Y-F, Masui H, Wu X-H, Heying B, Speck JS, Mishra UK, DenBaars SP: Metalorganic chemical vapor deposition growth of high optical quality and high mobility GaN. *J Electron Mater* 24, 1707–1709 (1995)

Kim D, Libon IH, Voelkmann C, Shen YR, Petrova-Koch V: Multiphoton photoluminescence from GaN with tunale picosecond pulses. *Phys Rev* B 55, 4907–4909 (1997)

Kishida H, Hasegawa T, Iwasa Y, Koda T, Tokura Y, Tachibana H, Matsumoto M, Wada S, Lay TT, Tashiro H: Electric-field-induced second-harmonic generation mediated by one-dimensional excitons in polysilanes. *Phys Rev* B 50, 7786–7792 (1994)

Liu A, Chuang S-L, Ning CZ: Piezoelectric field-enhanced second-order nonlinear optical susceptibilities in wurzite GaN/AlGaN quantum wells. *Appl Phys Lett* 76, 333–335 (2000)

Minsky MS, Fleischer SB, Abare AC, Bowers JE, Hu EL, Keller S, DenBaars SP: Characterization of high-quality InGaN/GaN multiquantum wells with time-resolved photoluminescence. *Appl Phys Lett* 72, 1066–1068 (1998)

Miragliotta J, Wickenden DK: Optical third-harmonic studies of the dispersion in $\chi^{(3)}$ for gallium nitride thin films on sapphire. *Phys Rev* B 50, 14960–14964 (1994)

Miragliotta J, Wickenden DK: Nonlinear electroreflectance from gallium nitride using optical second-harmonic generation. *Phys Rev* B 53, 1388–1397 (1996)

Mukai T, Narimatsu H, Nakamura S: Amber InGaN-based light-emitting diodes operable at high ambient temperature. *Jpn J Appl Phys* 37, L479–L481 (1998)

Nakamura S: The role of structural imperfections in InGaN-based blue light-emitting diodes and laser diodes. *Science* 281, 956–961 (1998a)

Nakamura S, Fasol G: *The Blue Laser Diode, GaN Based Light Emitters and Lasers.* Springer Verlag, Berlin, 1–333 (1997)

Nakamura S, Senoh M, Iwasa N, Nagahama S: High-brightness InGaN blue, green and yellow light-emitting diodes with quantum well structures. *Jpn J Appl Phys* 34, L797–L799 (1995)

Nakamura S, Senoh M, Nagahama S, Iwasa I, Yamada T, Matsushita T, Kiyoku H, Sugimoto Y, Kozaki T, Umemoto H, Sano M, Chocho K: High-power, long-lifetime InGaN/GaN/AlGaN-based laser diodes grown on pure GaN substrate. *Jpn J Appl Phys* 37, L309–L312 (1998b)

Nakamura S, Senoh M, Nagahama S, Matsushita T, Kiyoku H, Sugimoto Y, Kozaki T, Umemoto H, Sano M, Mukai T: Violet InGaN/GaN/AlGaN-based laser diodes operable at 50°C with a fundamental transverse mode. *Jpn J Appl Phys* 38, L226–L229 (1999)

Qui CH, Hoggatt C, Melton W, Leksono MW, Pankove JI: Study of defect states in GaN films by photoconductivity measurement. *Appl Phys Lett* 66, 2712–2714 (1995)

Redfield D, Aframowitz MA: The direct absorption edge in covalent solids. *Appl Phys Lett* 11, 138–140 (1967)

Riblet P, Hirayama H, Kinoshita A, Hirata A, Sugano T, Aoyagi Y: Determination of photoluminescence mechanism in InGaN quantum wells. *Appl Phys Lett* 75, 2241–2243 (1999)

Schmidt H, Abare AC, Bowers JE, DenBaars SP, Imamoglu A: Large interband second-order susceptibilities in InGaN/GaN quantum wells. *Appl Phys Lett* 75, 3611–3613 (1999)

Schmidt TJ, Cho Y-H, Gainer GH, Song JJ, Keller S, Mishra UK, DenBaars SP: Energy selective optically pumped stimulated emission from InGaN/GaN multiple quantum wells. *Appl Phys Lett* 73, 560–562 (1998a)

Schmidt TJ, Cho Y-H, Gainer GH, Song JJ, Keller S, Mishra UK, DenBaars SP: Pump-probe spectroscopy of band tail states in metalorganic chemical vapor deposition-grown InGaN. *Appl Phys Lett* 73, 1892–1894 (1998b)

Shen YR: *The Principles of Nonlinear Optics*. John Wiley & Sons, New York (1984)

Skromme BJ, Zhao H, Wang D, Kong HS, Leonard MT, Bulman GE, Molnar BJ: Strain determination in heteroepitaxial GaN. *Appl Phys Lett* 71, 829–831 (1997)

Sturge MD: Optical absorption of gallium arsenide between 0.6 and 2.75 eV. *Phys Rev* 127, 768–773 (1962)

Sun C-K, Liang J-C, Yu XY: Coherent acoustic phonon oscillations in semiconductor multiple quantum wells with piezoelectric fields. *Phys Rev Lett* 84, 179–182 (2000a)

Sun C-K, Liang J-C, Wang J-C, Kao F-J, Keller S, Mack MP, Mishra U, DenBaars SP: Two-photon absorption study of GaN. *Appl Phys Lett* 76, 439–441 (2000b)

Takeuchi T, Wetzel C, Yamaguchi S, Sakai H, Amano H, Akasaki I: Determination of piezoelectric fields in strained GaInN quantum wells using the quantum-confined Stark effect. *Appl Phys Lett* 73, 1691–1693 (1997)

Terhune RW, Maker PD, Savage CM: Optical harmonic generation in calcite. *Phys Rev Lett* 8, 404–406 (1962)

Vydra J, Eich M: Mapping of the lateral polar orientational distribution in second-order nonlinear thin films by scanning second-harmonic microscopy. *Appl Phys Lett* 72, 275–277 (1998)

Wang T, Nakagawa D, Wang J, Sugahara T, Sakai S: Photoluminescence investigation of InGaN/GaN single quantum well and multiple quantum wells. *Appl Phys Lett* 73, 3571–3573 (1998)

Ward JF, Elliott DS: Measurements of molecular hyperpolarizabilities for ethylene, butadiene, hexatriene, and benzene. *J Chem Phys* 69, 5438–5440 (1978)

Yu G, Wang G, Ishikawa H, Umeno M, Soga T, Egawa T, Watanabe J, Jimbo T: Optical properties of wurzite structure GaN on sapphire around fundamental absorption edge (0.78–4.77 eV) by spectroscopic ellipsometry and the optical transmission method. *Appl Phys Lett* 70, 3209–3211 (1997)

Zhang HY, He XH, Shih YH, Schurman M, Schurman M, Feng ZC, Stall RA: Waveguide study and refractive indices of GaN:Mg epitaxial film. *Opt Lett* 21, 1529–1531 (1996)